This is the peer reviewd version of the followng article:

Evidence of crystal packing effects in stabilizing high or low spin states of iron(II) complexes with functionalized 2,6-bis(pyrazol-1-yl)pyridine ligands / Bridonneau, N., Rigamonti, L., Poneti, G., Pinkowicz, D., Forni, A., Cornia, A.. - In: DALTON TRANSACTIONS. - ISSN 1477-9226. - 46:12(2017), pp. 4075-4085. [10.1039/c7dt00248c]

Terms of use:

The terms and conditions for the reuse of this version of the manuscript are specified in the publishing policy. For all terms of use and more information see the publisher's website.

16/10/2026 13:58

(Article begins on next page)

CrossMark
click for updates

View Article Online
View Journal

Dalton Transactions

Accepted Manuscript

This article can be cited before page numbers have been issued, to do this please use: N. Bridonneau, L. Rigamonti, G. Poneti, D. Pinkowicz, A. Forni and A. Cornia, *Dalton Trans.*, 2017, DOI: 10.1039/C7DT00248C.

This is an Accepted Manuscript, which has been through the Royal Society of Chemistry peer review process and has been accepted for publication.

Accepted Manuscripts are published online shortly after acceptance, before technical editing, formatting and proof reading. Using this free service, authors can make their results available to the community, in citable form, before we publish the edited article. We will replace this Accepted Manuscript with the edited and formatted Advance Article as soon as it is available.

You can find more information about Accepted Manuscripts in the author guidelines.

Please note that technical editing may introduce minor changes to the text and/or graphics, which may alter content. The journal's standard Terms & Conditions and the ethical guidelines, outlined in our author and reviewer resource centre, still apply. In no event shall the Royal Society of Chemistry be held responsible for any errors or omissions in this Accepted Manuscript or any consequences arising from the use of any information it contains.

ROYAL SOCIETY OF CHEMISTRY

rsc.li/dalton

View Article Online
DOI: 10.1039/C7DT00248C

Published on 22 February 2017. Downloaded by Fudan University on 22/02/2017 11:06:05.

Evidences of crystal packing effects in stabilizing high or low spin state of iron(II) complexes with functionalized 2,6-bis(pyrazol-1-yl)pyridine ligands†

Nathalie Bridonneau,[a] Luca Rigamonti,*[a] Giordano Poneti,[b,c] Dawid Pinkowicz,[d] Alessandra Forni[e] and Andrea Cornia[a]

[a] *Dipartimento di Scienze Chimiche e Geologiche, Università degli Studi di Modena e Reggio Emilia and INSTM RU of Modena and Reggio Emilia, via G. Campi 103, 41125 Modena, Italy; E-mail: luca.rigamonti@unimore.it*

[b] *Laboratory of Molecular Magnetism (LAMM), Dipartimento di Chimica 'Ugo Schiff', Università degli Studi di Firenze e INSTM RU of Firenze, via della Lastruccia 3-13, 50019 Sesto Fiorentino (FI), Italy*

[c] *Current address: Instituto de Química, Universidade Federal do Rio de Janeiro, 21941-909 Rio de Janeiro, Brazil*

[d] *Faculty of Chemistry, Jagiellonian University, Ingardena 3, 30-060 Kraków, Poland*

[e] *Consiglio Nazionale delle Ricerche (CNR), Istituto di Scienze e Tecnologie Molecolari (ISTM), via C. Golgi 19, 20133 Milano, Italy*

† Electronic supplementary information (ESI) available: experimental section with the synthesis and characterization of the ligands bpp-COOMe and bpp-triolH_3, crystal packing in **1** (**Fig. S1**) and **2**·MeCN (**Fig. S2**), hydrogen bonds in **1** (**Table S1**) and **2**·MeCN (**Table S2**), temperature dependence of the $\chi_M T$ product and isothermal field dependence of the magnetization at 1.8 K under different external pressures of **1** (**Fig. S3**), isothermal field dependence of the magnetization at 1.8, 2.5 and 4.5 K of **2** (**Fig. S4**), time dependence of the $\chi_M T$ product of **2** under 532 nm light irradiation at 10 K (**Fig. S5**), plots of the (U)M06/6-311+G(d) frontier orbitals mainly localized on the iron(II) centre of the $[Fe(bpp\text{-}R)_2]^{2+}$ cations (R = COOMe, triolH_3) in **1** and **2** at both spin states $S = 0$ and $S = 2$ (**Fig. S6**), Cartesian coordinates, electronic energies and NBO charges of the modelled bpp-R free ligands and $[Fe(bpp\text{-}R)_2]^{2+}$ cations (R = COOMe, triolH_3) in **1** and **2** in both spin states $S = 0$ and $S = 2$ (**Table S3**). For ESI and crystallographic data see DOI: 10.1039/***.

Abstract

Molecular structures and magnetic properties of the homoleptic iron(II) compounds $[Fe(bpp\text{-}COOMe)_2](ClO_4)_2$ (**1**) and $[Fe(bpp\text{-}triolH_3)_2](ClO_4)_2$ (**2**) have been investigated to ascertain their

Dalton Transactions Accepted Manuscript

View Article Online
DOI: 10.1039/C7DT00248C

Published on 22 February 2017. Downloaded by Fudan University on 22/02/2017 11:06:05.

spin crossover (SCO) behaviour. In these hexacoordinated complexes, the bpp (2,6-bis(pyrazol-1-yl)pyridine) ligands adopt a *mer-mer* coordination mode and carry COOMe or $C(O)NHC(CH_2OH)_3$ *para* substituents, respectively, on the central pyridyl ring. In spite of the almost equal donor power of the ligands to the iron(II) centre, the two compounds feature different spin state configurations at room temperature. Compound **1** displays a highly-distorted octahedral environment around the iron(II) centre, which adopts a high spin (HS) state at all temperatures, even under an external applied pressure up to 1.0 GPa. By contrast, **2** is characterized by a more regular octahedral coordination around the metal ion and exhibits a low spin (LS) configuration at or below room temperature. However, it shows a thermally-induced SCO behaviour at $T > 400$ K, along with Light-Induced Excited Spin State Trapping (LIESST) at low temperature, with $T_{LIESST} = 38$ K. Since DFT (U)M06/6-311+G(d) geometry optimizations *in vacuo* indicate that both complexes should adopt a HS state and a highly-distorted coordination geometry, the stabilization of a LS configuration in **2** is ultimately ascribed to the effect of intermolecular hydrogen bonds, which align the $[Fe(bpp\text{-}triolH_3)_2]^{2+}$ cations in 1D chains and impart profound differences in the geometric arrangement of the ligands.

Introduction

Spin crossover (SCO) materials have been extensively investigated in the last years, since the reversible control of their spin state by external stimuli holds promises for application in information processing and data storage devices or molecular switches.[1,2] Special interest has been focussed on compounds that show persistent change of magnetization upon light irradiation. The so-called LIESST (Light-Induced Excited Spin State Trapping) effect, first demonstrated by Hauser et al,[3] consists in the photo-induced conversion of a low spin (LS) state to a metastable high spin (HS) state at cryogenic temperatures. The LIESST effect has been mostly studied in iron(II) complexes,[3–8] although iron(III)[9] or molybdenum(IV)[10] can also exhibit a similar behaviour. Pressure is another important external stimulus used to shift the spin equilibrium: due to the larger size of the HS centre compared to the LS one, the application of an external pressure favours a LS configuration,[11,12] additionally increasing the SCO transition temperature.[13]

2,6-Bis(pyrazol-1-yl)pyridine (1-bpp), 2,6-bis(pyrazol-3-yl)pyridine (3-bpp) and their differently-substituted derivatives, hereafter called generically bpp ligands, afford $[Fe^{II}(bpp)_2](X)_2$ (X^- = anion) complexes that can exhibit SCO behaviour (Scheme 1).[7,8,14,15] Depending on functionalization and counterion, gradual to abrupt spin conversions are observed, with associated

Dalton Transactions Accepted Manuscript

View Article Online
DOI: 10.1039/C7DT00248C

Published on 22 February 2017. Downloaded by Fudan University on 22/02/2017 11:06:05.

transition temperatures ($T_{½}$) ranging from 100 K up to room temperature and above. What is clear is that the SCO ability is primarily governed by the distortion of the coordination sphere as described by the angles ϕ and θ,[7] depicted in Scheme 1, together with the clamp angle ψ.[16] Notice that the most regular geometry, achieved with $\phi = 180°$ and $\theta = 90°$, still exhibits departures from perfect octahedral symmetry due to the intrinsic shape of bpp ligands, which imposes a clamp angle $\psi < 180°$. Even though the two distortion angles can occur independently of each other,[7,8] their combination is probably the key factor determining the existence of SCO behaviour. Previous surveys[7,8] indicated that derivatives with $\phi \geq 172°$ and $\theta \geq 76°$ (low distortion) in their HS state can easily rearrange to the more regular geometry typical of the LS state and usually show spin conversion upon cooling. Most of highly distorted complexes ($\phi < 172°$ and $\theta < 76°$), on the other hand, remain trapped in their HS state at all temperatures in the solid state and therefore do not exhibit SCO behaviour.[7,8] The two distortion indices Σ (local angular distortions of the octahedral donor set N_6) and Θ (degree of trigonal distortion of the coordination geometry from an octahedron towards a trigonal prism) can be also used as probes of the spin state.[17] They are lower for the LS compounds than for the HS ones, confirming that LS complexes have more regular coordination geometries.[7] The values of ϕ and θ (and consequently of Σ and Θ) are mainly affected by Jahn-Teller effect,[18] and in the second place by crystal packing. This is clearly shown by the derivatives $[Fe(1\text{-bpp})_2](X)_2$, whose coordination distortion varies by changing the counterion X.[7,18,19] LIESST effect was reported as well for this family of compounds,[20] since this type of ligands usually promote adequate iron(II) geometries that lead to long lifetimes of the photo-induced metastable state.[21]

Among all bpp ligands, our attention has been focused on derivatives of 1-bpp, hereafter called bpp-R, in which the R substituent is introduced in the *para* position of the central pyridyl ring, hence approximately along the N{py}–Fe–N{py} bond direction and the distortion angle ϕ. The R groups used in the past years range from alkyl,[22] halogen[23,24] alcohol,[22,25] thioether,[24,26] pyridine,[27,28] aldehyde,[29] cyano[30] and carboxylic acid[31] to ferrocene,[32] guanidine or cytosine,[33] tetrathiafulvalene,[34] pyrene,[35] C≡C–R (R = H, $SiMe_3$, Br)[36] TEMPO[37] and *Z*-to-*E* photoisomerizable C=C–Ar[38] fragments. Given this large pool of available derivatives, a unified treatment of the relationship between the electronic nature of R and the SCO properties shown by the iron(II) complexes in solution has been recently proposed.[39] The situation is more puzzling when analysing the effect of intermolecular contacts on the magnetic behaviour in the solid state. Weak van der Waals interactions,[22] π-π stacking[35] or relatively strong hydrogen bonds,[27,31] together with the steric

Dalton Transactions Accepted Manuscript

View Article Online
DOI: 10.1039/C7DT00248C

Published on 22 February 2017. Downloaded by Fudan University on 22/02/2017 11:06:05.

hindrance of the substituent itself, can in fact come into play and further affect the distortion angles and then the relative stability of the high or low spin state. The most extremely distorted structures are often associated with secondary contacts in the crystal between the complex and the neighboring anions,[8] but when cations pack into the so-called "terpyridine embrace lattice",[17] spin transition is still observable.[22]

We here report the structural and magnetic properties of two new compounds belonging to the $[Fe(bpp\text{-}R)_2](X)_2$ family, namely $[Fe(bpp\text{-}COOMe)_2](ClO_4)_2$ (**1**) and $[Fe(bpp\text{-}triolH_3)_2](ClO_4)_2$ (**2**), where the two moieties COOMe and $C(O)NHC(CH_2OH)_3$ (= $triolH_3$), respectively (Scheme 1), are unable (**1**) or able (**2**) to give relatively strong H bonds in condensed phase. The two tridentate bpp-R ligands coordinate the iron(II) ion with a meridional-meridional (*mer-mer*) configuration giving an octahedral coordination environment, but with different distortion degrees in **1** and **2**, and consequently different spin states at room temperature. The role of crystal packing and intermolecular contacts is here analysed and discussed with the help of pressure-dependent experiments, photo-magnetic studies and DFT calculations.

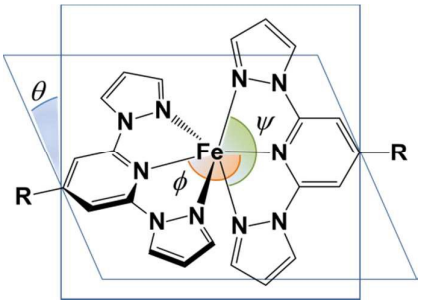

Scheme 1 Molecular scheme of $[Fe(bpp\text{-}R)_2]^{2+}$ complexes, highlighting the two distortion components (θ and ϕ angles) responsible for SCO behaviour modulation, together with the clamp angle ψ. In this paper, R = COOMe (**1**) and $C(O)NHC(CH_2OH)_3$ or $triolH_3$ (**2**).

Experimental

General information

Unless otherwise stated, all chemicals were of reagent grade and used as received. Diethyl ether (Et_2O) was predried over $CaCl_2$ overnight and distilled from sodium benzophenone under N_2 before use. Acetonitrile (MeCN) was treated with CaH_2 and then distilled under N_2. Elemental analyses were recorded using a Carlo Erba EA1110 CHNS-O automatic analyser. IR spectra were recorded as KBr discs using a Jasco FTIR-4700LE spectrophotometer with a 2 cm^{-1} resolution. Further

Dalton Transactions Accepted Manuscript

View Article Online
DOI: 10.1039/C7DT00248C

Published on 22 February 2017. Downloaded by Fudan University on 22/02/2017 11:06:05.

general details and the syntheses of the ligands are reported in the ESI.† ***Caution!*** Perchlorate salts are explosive in nature and should be handled in small amounts and carefully.

Synthesis of metal complexes

[Fe(bpp-COOMe)$_2$](ClO$_4$)$_2$ (1). Solid Fe(ClO$_4$)$_2$·6H$_2$O (24.1 mg, 0.0664 mmol) was added to a suspension of bpp-COOMe (34.8 mg, 0.129 mmol) in MeCN (3 mL) causing the immediate dissolution of the ligand and a colour change to red-purple upon formation of the desired complex. After 30 minutes stirring, the solution was filtered to eliminate undissolved material and put in vapour diffusion with Et$_2$O (5 mL). Diffusion was complete in about one week and the X-ray quality red crystalline product was collected by filtration, quickly washed with Et$_2$O:MeCN (2:1 v/v) and dried in vacuum. Yield: 35.7 mg (69.6%). Anal (%) Calcd for $C_{26}H_{22}Cl_2FeN_{10}O_{12}$ (793.26): C 39.37, H 2.80, N 17.66. Found: C 39.25, H 2.72, N 17.97. FT-IR (KBr, cm^{-1}): 1737s (νC=O ester), 1631m + 1579s + 1522s + 1404s (νC=C, νC=N), 1459s + 1444m (δC–H), 1095s (νClO$_4^-$), 1058s (νC–O).

[Fe(bpp-triolH$_3$)$_2$](ClO$_4$)$_2$ (2). This compound was prepared and isolated with the same method described for **1**, starting from Fe(ClO$_4$)$_2$·6H$_2$O (19.3 mg, 0.0532 mmol) and bpp-triolH$_3$ (40.0 mg, 0.112 mmol). Once removed from the mother liquor, the crystals (**2**·MeCN) undergo quick solvent loss. Yield: 21.0 mg (40.6%). Anal (%) Calcd for $C_{32}H_{36}Cl_2FeN_{12}O_{16}$ (971.45): C 39.56, H 3.74, N 17.30. Found: C 39.47, H 4.00, N 17.66. FT-IR (KBr, cm^{-1}): 3407br + 3240sh (νO–H, νN–H), 1663s (νC=O amide), 1630m + 1570s + 1525s + 1498s + 1407s (νC=C, νC=N), 1471s (δC–H), 1103s (νClO$_4^-$), 1056m (νC–O).

X-ray crystal structure determination

Single-crystal X-ray diffraction studies were carried out on **1** and **2**·MeCN with a four-circle Bruker X8-APEX diffractometer equipped with a Mo-Kα generator (λ = 0.71073 Å), an area detector and a Kryo-Flex cryostat, and controlled by Bruker-Nonius X8APEX software. The selected individual of **2**·MeCN was taken directly from the MeCN/Et$_2$O mother liquor, rapidly mounted on a glass fiber and cooled in the nitrogen flux of the cryostat. The structures were solved by direct methods using the SIR92[40] program and refined on F_o^2 by full-matrix least-squares methods using the SHELXL-2014/7[41] software; both programs are implemented in the WINGX[42] v2014.1 package. The program Mercury 3.8[43] was used for graphics. Crystal structure data and refinement parameters for **1** and **2**·MeCN are gathered in Table 1. Disorder effects were resolved only in the structure of **2**·MeCN,

Dalton Transactions Accepted Manuscript

View Article Online
DOI: 10.1039/C7DT00248C

Published on 22 February 2017. Downloaded by Fudan University on 22/02/2017 11:06:05.

where they affected one OH group *per* ligand (O4A:O4B 0.586(3):0.414(3); O8A:O8B:O8C 0.586(3):0.250(3):0.164(3)), one perchlorate anion (Cl2A:Cl2B 0.531(7):0.469(7)) and the interstitial acetonitrile molecule (0.589(9):0.411(9)). These disordered moieties were refined with restraints on their geometrical and displacement parameters. All non-hydrogen atoms were treated anisotropically, except for disordered atoms with occupancy < 0.25. Perchlorate anions were modelled as variable-metrics tetrahedra, with allowed deviations of 0.01 and 0.02 Å for Cl–O and O···O distances, respectively, and RIGU/ISOR restraints on displacement parameters. The hydrogen atoms of **1** were located in ΔF maps and fully refined with isotropic displacement parameters (IDPs). The hydrogen atoms of **2**·MeCN were idealized and treated as riding contributors with IDPs constrained to be 50% (for CH_3) or 20% higher than those of the parent atoms. OH groups were either subject to torsion angle refinement (AFIX 147) or placed in a staggered conformation so as to afford the best hydrogen bond (AFIX 83). In **2**·MeCN, a large (ca. 4 $e^-/Å^3$) electron density residual was found close to the C31–O7 hydroxymethyl group, at 1.36 Å from C31. When this peak was assigned to the minority (ca. 15%) component of a disordered C–O group, an unphysically short (2.19 Å) intermolecular contact was produced with C25, belonging to a non-disordered hydroxymethyl group. This suggests that the residual electron density peak might be an artefact related to unresolvable crystal twinning or other so-far unidentified causes. The final *R* indices are consequently high, but the structural model is otherwise satisfactory for the purpose of this study. CCDC 1522449 and 1522450 contain the supplementary crystallographic data for this paper. These data can be obtained free of charge from the Cambridge Crystallographic Data Centre via www.ccdc.cam.ac.uk/data_request/cif.

Magnetic measurements

Magnetization measurements were carried out on 7.38 and 8.66 mg pelletized polycrystalline samples of **1** and **2**, respectively, using a Quantum Design MPMS SQUID magnetometer equipped with a 5 T magnet. The temperature dependence of molar magnetic susceptibility (χ_M) was followed from 1.8 to 300 (400) K for **1** (**2**) with an applied field H_{DC} = 10 kOe at $T \geq 35$ K and 1 kOe at $T <$ 35 K so as to reduce magnetic saturation effects. The field dependence of molar magnetization (M_M) was also evaluated at 1.8, 2.5 and 4.5 K with applied field up to 50 kOe. Magnetic data were corrected for the sample holder contribution and for the sample diamagnetism (-421×10^{-6} and -392×10^{-6} emu mol^{-1} for **1** and **2**, respectively, calculated from Pascal's constants[44]).

Dalton Transactions Accepted Manuscript

View Article Online
DOI: 10.1039/C7DT00248C

Published on 22 February 2017. Downloaded by Fudan University on 22/02/2017 11:06:05.

Magnetic measurements under pressure on **1** were performed using Quantum Design MPMS3 magnetometer equipped with a 7 T magnet. A polycrystalline sample of 9.1 mg was loaded into the CuBe piston-cylinder type high pressure capsule cell (HMD, Japan). Daphne 7373 oil was used as a pressure-transmitting medium hydrostatic up to 1.2 GPa. The actual pressure (p) in the sample chamber at low temperature was determined with 0.02 GPa accuracy from the linear pressure dependence of the superconducting transition temperature (T_c) of high-purity lead (dT_c/dp = 0.379 K GPa^{-1}). The residual field of the magnet was cancelled before each measurement using the magnet reset option. The magnetic data were corrected for the background of the pressure cell filled with oil. The temperature dependence of χ_M was followed from 1.8 to 300 K by applying H_{DC} = 1 kOe, and the field dependence of M_M was then evaluated at 1.8 K with field up to 70 kOe under different applied pressures up to 1.00 GPa. Magnetic data were corrected with the same diamagnetic sample contribution reported above.

Photo-magnetic measurements were carried out on a pelletized mixture of polycrystalline **2** (~ 0.5 mg) and powdered KBr so as to facilitate light penetration (the actual Fe content was evaluated by scaling the magnetic moment on that of the heavier sample of pure **2** used for regular measurements). Irradiation experiments were performed using a 532 nm laser beam with the CW laser diode coupled to an optical fibre inserted in the sample space through a hollow sample rod. The beam was collimated on the sample by means of an aspheric lens, yielding a radiant power on the sample of about 2 mW cm^{-2}. T_{LIESST} measurement consisted of monitoring the temperature featuring a minimum in the d($\chi_M T$)/dT curve, after reaching the photo-stationary limit at 10 K, switching the laser off and warming up the sample at a rate of 0.3 K min^{-1}. Magnetic moments were corrected for the diamagnetic contribution of KBr and the sample holder (independently measured in the same range of field and temperature) as well as for the intrinsic diamagnetism of the sample (see above).

Computational details

In vacuo DFT calculations were performed on the cations [Fe(bpp-R)$_2$]$^{2+}$ of **1** and **2** using Gaussian 09,[45] at the (U)M06/6-311+G(d) and (U)M06/6-31+G(d) levels of theory. The M06 functional[46] was adopted owing to its optimal performance in treating organometallic systems.[46] (U)M06/6-311+G(d) geometry optimizations were performed in both S = 0 and S = 2 spin states, starting from both the distorted and undistorted geometries around the iron(II) ion as provided by X-ray experiments. For each complex, optimizations with such four starting guesses ended up in only two minima, i.e., the distorted HS and the undistorted LS states, the former being the most stable one for

Dalton Transactions Accepted Manuscript

View Article Online
DOI: 10.1039/C7DT00248C

Published on 22 February 2017. Downloaded by Fudan University on 22/02/2017 11:06:05.

both **1** and **2**. Frequencies calculations at the same level of theory confirmed that the optimized S = 0 structures were true minima, while spurious imaginary frequencies were obtained for the optimized structures with S = 2. Such negative frequencies were eliminated only by increasing the grid size up to 99,590 (Grid = UltraFine option in Gaussian 09) and reducing the basis set to 6-31+G(d), with no significant change in the optimized parameters. Thermal analysis was then performed at 298 K at (U)M06/6-31+G(d) level of theory. The Natural Bond Orbital (NBO) analysis[47] was used for evaluating the atomic charges of both bpp-R ligands and (U)M06/6-311+G(d) structurally-optimized complex cations (Tables with Cartesian coordinates, electronic energies and NBO charges of the two ligands and of the optimized complexes in the two spin configurations are reported as ESI†).

Table 1 Crystallographic data and refinement parameters for **1** and **2**·MeCN.

	1	**2**·MeCN
formula	$C_{26}H_{22}Cl_2FeN_{10}O_{12}$	$C_{34}H_{39}Cl_2FeN_{13}O_{16}$
formula weight	793.28	1012.53
crystal system	monoclinic	monoclinic
space group	$C2/c$ (n. 15)	$P2_1/n$ (n. 14)
T, K	115(2)	140(2)
a, Å	23.476(3)	14.0675(10)
b, Å	10.3734(11)	16.2407(11)
c, Å	15.7959(18)	18.2548(11)
β, °	127.074(2)	101.045(2)
V, Å^3	3069.1(6)	4093.3(5)
Z	4	4
ρ_{calcd}, g cm^{-3}	1.717	1.643
μ, mm^{-1}	0.749	0.590
crystal size, mm^3	0.39 × 0.35 × 0.21	0.26 × 0.20 × 0.12
$2\theta_{max}$, °	64.04	52.99
collected/indep reflns	21845/5317	40776/8447
R_{int}	0.0311	0.0580
restraints/parameters	0/275	179/679
R_1, wR_2 ($I > 2\sigma(I)$)	0.0318, 0.0872	0.0928, 0.2568
R_1, wR_2 (all data)	0.0350, 0.0898	0.1295, 0.2869
goodness-of-fit	1.031	1.121

Dalton Transactions Accepted Manuscript

View Article Online
DOI: 10.1039/C7DT00248C

Published on 22 February 2017. Downloaded by Fudan University on 22/02/2017 11:06:05.

Results

Synthesis of ligands and formation of the complexes

The synthesis of bpp-triolH_3 was based on a four-step reaction, which started from commercially available citrazinic acid and involved bpp-COOMe as an intermediate (Scheme 2). The detailed synthetic conditions described in the ESI† are based on previous important work by Halcrow *et al.*[14,48] and, more recently, by Coronado *et al.*,[31,49] in which the ligands bpp-COOMe[27] and bpp-triolH_3[49] were separately reported. Methyl 2,6-dichloroisonicotinate was first synthesized according to literature procedure[33,51–54] by reacting citrazinic acid with phosphorous oxychloride in the presence of ammonium chloride and heating the reaction mixture overnight at 140 °C. After cooling down to room temperature, cold methanol was added and the compound was precipitated by addition of aqueous K_2CO_3. The acid bpp-COOH was obtained[27,31] by prolonged heating of methyl 2,6-dichloroisonicotinate with pyrazole and NaH in diglyme, followed by acid workup. The methyl ester bpp-COOMe was then prepared by standard methods and reacted with tris(hydroxymethyl)aminomethane in DMSO at room temperature in the presence of K_2CO_3. After filtration of the excess of the potassium salt and removal of the solvent in vacuo, treatment of the yellow oily residue with $CHCl_3$/*n*-hexane gave bpp-triolH_3 as a white powder in considerably improved yield as compared with the available literature procedure (78 vs. 38%).[49] All products were achieved in good yields on the gram scale leading to a remarkable overall yield of 46% for the four-step procedure.

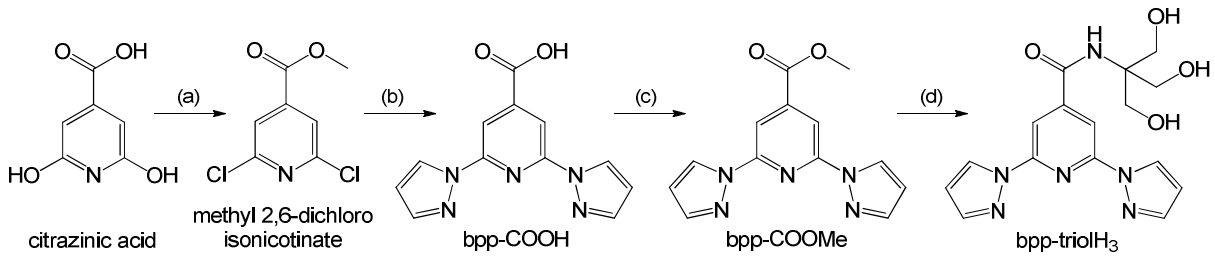

Scheme 2 (a) *i*) $POCl_3$, 140 °C (overnight) *ii*) MeOH (86%); (b) pyrazole, NaH, diglyme, 140 °C (5 days) (83%); (c) $SOCl_2$, MeOH (82%); (d) tris(hydroxymethyl)aminomethane, DMSO, K_2CO_3 (78%).

The synthesis of the metal complexes **1** and **2** was conveniently carried out by adding the metal perchlorate salt to a suspension of the bpp-R ligands in MeCN, which caused immediate dissolution of the ligand and a concomitant colour change to red-purple. Vapour diffusion of Et_2O in the

Dalton Transactions Accepted Manuscript

View Article Online
DOI: 10.1039/C7DT00248C

Published on 22 February 2017. Downloaded by Fudan University on 22/02/2017 11:06:05.

filtered solution afforded the desired products in reasonable yields as red X-ray quality crystals within a week. The infrared spectrum of **1** shows a slight blue-shift of the ester C=O stretching band from 1732 cm^{-1} in the free ligand to 1737 cm^{-1}. By contrast, the amide C=O stretching band in **2** undergoes a red-shift from 1671 to 1663 cm^{-1} upon complexation. νO–H and νN–H vibration modes in **2** appear as a broad intense band centred at 3400 cm^{-1} accompanied by a shoulder at 3240 cm^{-1} that extends down to 2700 cm^{-1}. This pattern is suggestive of a hydrogen bond network involving O–H and N–H groups in the solid state (see below). The perchlorate stretching is present in both spectra as a broad signal centred at 1100 cm^{-1}, as expected for ClO_4^- anions in T_d symmetry.[54]

Crystal and molecular structures

Compound **1** crystallizes in monoclinic *C*2/*c* space group with four formula units per unit cell. The iron(II) ion sits on a twofold crystallographic axis and the asymmetric unit contains half mononuclear complex and one perchlorate anion. By consequence, the $[Fe(bpp\text{-}COOMe)_2]^{2+}$ complex has crystallographically-imposed twofold symmetry (Fig. 1). Selected geometrical parameters of the coordination sphere at 115(2) K are gathered in Table 2. The clearest aspect in the molecular structure of this hexacoordinated iron(II) complex is the distortion of the octahedral coordination environment, as described by the *trans*-N{py}–Fe–N{py} angle ϕ = 158.77(5)° and by the dihedral (twisting) angle between the two ligands θ = 80.738(12)°. The clamp angle ψ = 146.33(3)° reflects the coordination of the bpp-COOMe ligands with long Fe–N distances (2.14–2.20 Å) that are characteristic of the HS state[8] (see below). The same conclusion can be drawn by inspecting the distortion index Σ, whose value (155.7°) lies well within the range typically exhibited by HS complexes (140–200°).[7] The coordination mode is also quite asymmetric, with a difference in the Fe–N bond distances of the two pyrazolyl arms of about 0.03 Å, and a shorter Fe–N bond length with the central pyridyl ring.

The two shortest intermolecular interactions between $[Fe(bpp\text{-}COOMe)_2]^{2+}$ cations involve two pyrazolyl C–H groups: one occurs with the carbonyl group (C1(H1)···O1 = 3.2704(15) Å, C1–H1···O1 = 153.44(15)° (Fig. 1) and leads to an intermolecular Fe···Fe distance of 9.632 Å. The second one involves the pyrazolyl ring of an adjacent molecule (C10(H10)···centroid (N1C1C2C3N4) = 3.44 Å, C10–H10···centroid(N1C1C2C3N4) = 149°) (Fig. 1) with an intermolecular Fe···Fe distance of 8.480 Å. Perchlorate anions are located in the voids between cations and all their oxygen atoms are involved in weak C–H···O interactions (ESI, Fig. S1†).

Dalton Transactions Accepted Manuscript

View Article Online
DOI: 10.1039/C7DT00248C

Published on 22 February 2017. Downloaded by Fudan University on 22/02/2017 11:06:05.

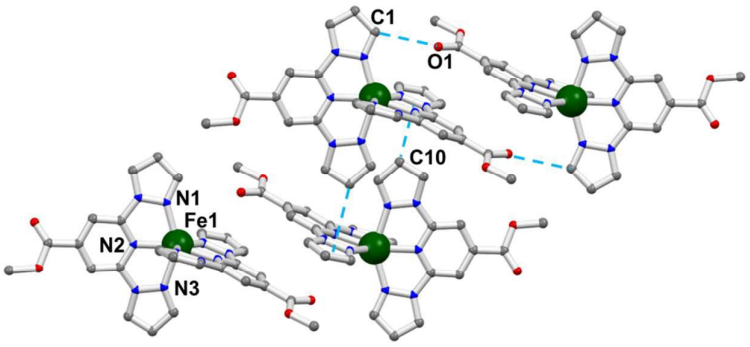

Fig. 1 Molecular structure and crystal packing of the cation $[Fe(bpp\text{-}COOMe)_2]^{2+}$ in **1** with selected atom labels; intermolecular contacts are depicted as light blue dashes (colour code: Fe = dark green, O = red, N = blue, C = grey, H atoms and ClO_4^- anions omitted for clarity).

Table 2 Bond distances (Å), angles (°) and distortion indices (°) of **1** from single-crystal X-ray diffraction and computational studies on the cation $[Fe(bpp\text{-}COOMe)_2]^{2+}$ in both HS ($S = 2$) and LS ($S = 0$) states.

	experimental	HS ($S = 2$)	LS ($S = 0$)
Fe1–N1	2.1643(10)	2.174	1.996
Fe1–N2 (py)	2.1366(9)	2.150	1.914
Fe1–N3	2.1932(10)	2.200	1.996
r_{Fe-N} [a]	2.165	2.175	1.969
N1–Fe1–N2	73.38(3)	73.28	79.93
N2–Fe1–N3	73.27(3)	72.85	79.85
N1–Fe1–N3 (ψ)	146.33(3)	144.87	159.78
N2–Fe1–N2' [b] (ϕ)	158.77(5)	158.44	179.55
θ [c]	80.738(12)	77.86	90.00
Σ [d]	155.7	160.5	88.0
Θ [d]	479	500	288

[a] average Fe–N distance; [b] primed atom is obtained from unprimed one through twofold rotation; [c] dihedral angle between the two ligands (the plane of each ligand was defined as the least-squares plane through its sixteen aromatic C/N atoms); [d] see ref. 7 for its definition.

Compound **2**·MeCN crystallizes in monoclinic $P2_1/n$ space group, with four formula units per unit cell. The asymmetric unit comprises one mononuclear complex, two perchlorate anions and one interstitial MeCN molecule (Fig. 2). Selected coordination parameters at 140(2) K, reported in Table 3, show that the $[Fe(bpp\text{-}triolH_3)_2]^{2+}$ cation features a much smaller distortion as compared

Dalton Transactions Accepted Manuscript

View Article Online
DOI: 10.1039/C7DT00248C

Published on 22 February 2017. Downloaded by Fudan University on 22/02/2017 11:06:05.

with **1**. Its angular parameters ϕ = 179.30(15)° and θ = 87.414(34)° are indeed very close to the ideal values for a regular octahedron. The clamp angles ψ_1 and ψ_2 of the two crystallographically-independent bpp-triolH_3 ligands are very similar to each other and close to 160°. The Fe–N distances range from 1.89 to 1.97 Å, with the central pyridyl ring still forming the shortest coordination bond. These bond lengths and the low value of the distortion index Σ (85.0°) are characteristic of a LS state.[8] The two Fe–N bonds with pyrazolyl nitrogen atoms are now of equal length within experimental error and the FeN_6 chromophore thus closely approaches D_{2d} symmetry.

The partially-disordered OH groups of the ligands give rise to a series of intra- and inter-molecular hydrogen bonds (Fig. 2 and ESI, Table S2†). One full-occupancy OH group per ligand is intramolecularly H-bonded to the carbonyl oxygen (O2···O1 = 2.770(5) Å, O2–H···O1 = 129.8°; O7···O5 = 2.747(5) Å, O7–H···O5 = 141.3°). The majority component of a disordered OH group is also involved in an intramolecular H bond within the trimethylol portion of the ligand (O8A···O6 = 2.658(8) Å, O8A–H···O6 = 140.4°). Intermolecular H bonds link the cations into approximately linear chains (O4A···O7 = 2.671(7) Å, O4A–H···O7 = 163.0°) and provide interconnections between chains (N11···O8A = 2.846(7) Å, N11–H···O8A = 154.2°). The two remaining OH groups are involved in H bonds with the perchlorate anions (O3···O11 = 2.902(10) Å, O3–H···O11 = 155.4°; O6···O12 = 2.769(7) Å, O6–H···O12 = 171.1°). The interstitial acetonitrile molecule is disordered and is only weakly bound to the surrounding cations and anions. It simply fills the voids in the crystal lattice (ESI, Fig. S2†) and is in fact rapidly lost once the crystals are removed from their mother liquor. Within this crystal packing, the shortest Fe···Fe separation is 8.702 Å, hence very close to that found in **1**.

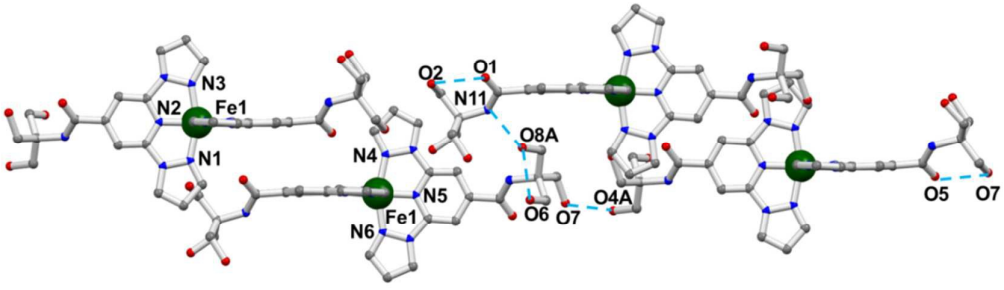

Fig. 2 Molecular structure and crystal packing of the cation $[Fe(bpp\text{-}triolH_3)_2]^{2+}$ in **2**·MeCN with selected atom labels; H bonds are depicted as light blue dashes (colour code: Fe = dark green, O = red, N = blue, C = grey; H, ClO_4^- anions and acetonitrile omitted for clarity; only the main components of the disordered OH groups are drawn).

Dalton Transactions Accepted Manuscript

View Article Online
DOI: 10.1039/C7DT00248C

Published on 22 February 2017. Downloaded by Fudan University on 22/02/2017 11:06:05.

Table 3 Bond distances (Å), angles (°) and distortion indices (°) of **2** from single-crystal X-ray diffraction and computational studies on the cation $[Fe(bpp\text{-}triolH_3)_2]^{2+}$ in both LS ($S = 0$) and HS ($S = 2$) states.

	experimental	LS ($S = 0$)	HS ($S = 2$)
Fe1–N1	1.973(4)	1.997	2.202
Fe1–N2 (py)	1.894(4)	1.916	2.144
Fe1–N3	1.967(4)	1.997	2.177
Fe1–N4	1.972(3)	–[a]	2.200
Fe1–N5 (py)	1.895(4)	–[a]	2.146
Fe1–N6	1.965(4)	–[a]	2.179
$r_{Fe–N}$[b]	1.944	1.970	2.175
N1–Fe1–N2	80.12(14)	79.74	73.00
N2–Fe1–N3	80.36(14)	79.87	73.33
N1–Fe1–N3 (ψ_1)	160.48(14)	159.61	145.49
N4–Fe1–N5	80.43(14)	–[a]	72.96
N5–Fe1–N6	79.91(14)	–[a]	73.22
N4–Fe1–N6 (ψ_2)	160.34(14)	–[a]	144.97
N2–Fe1–N5 (ϕ)	179.30(15)	178.58	160.11
θ[c]	87.414(34)	89.49	79.55
Σ[d]	85.0	88.7	157.8
Θ[d]	292	290	495

[a] only symmetry-unique parameters are given for the computed structures; [b] average Fe–N distance; [c] dihedral angle between the two ligands (the plane of each ligand was defined as the least-squares plane through its sixteen aromatic C/N atoms); [d] see ref. 7 for its definition.

Compound **1** belongs to the small number of HS derivatives with $\phi < 160°$, which in few cases approaches 150°,[34,38a] and thus does not fulfil the condition suggested for SCO to be possible ($\phi > 172°$).[8] Notice, however, that the compounds $[Fe(bpp\text{-}Me)_2](ClO_4)_2$ ($\phi = 163.7°$, $\theta = 89.5°$)[22] and $[Fe(bpp\text{-}E\text{-}C{=}C–C_6H_5)_2](BF_4)_2$·acetone ($\phi = 161.9$, $\theta = 73.0$)[38c] were both shown to exhibit SCO in spite of their low ϕ values. Since the θ parameter in **1** is definitely more favourable than in $[Fe(bpp\text{-}E\text{-}C{=}C–C_6H_5)_2](BF_4)_2$·acetone[38c] and well above the threshold value for SCO (76°), **1** earns a chance for showing SCO.

By contrast, **2**, with its approximate D_{2d} symmetry, is a perfect candidate for undergoing thermally- and light-induced SCO. In particular, it bears overall structural resemblance and similar distortion parameters to the SCO derivatives $[Fe(bpp\text{-}pPy)_2H](ClO_4)_3$ ($T_{½}$ = 286 K)[27] (bpp-pPy = 2',6'-bis(pyrazol-1-yl)-4,4'-bipyridine) and $Fe(bpp\text{-}COOH)_2](ClO_4)_2$ ($T_{½}$ = 382 K),[31] in which

Dalton Transactions Accepted Manuscript

View Article Online
DOI: 10.1039/C7DT00248C

Published on 22 February 2017. Downloaded by Fudan University on 22/02/2017 11:06:05.

complex cations also interact via H bonds and form supramolecular chains (see below for more details). In order to ascertain the possible occurrence of SCO, we undertook magnetic and photomagnetic studies on **1** and **2**.

Magnetic properties

The temperature dependence of the low-field molar magnetic susceptibility of **1** is reported in Fig. 3 as a $\chi_M T$ vs. T plot along with the isothermal field dependence of the molar magnetization, M_M, up to 5 T at 1.8, 2.5 and 5.0 K. At 300 K the $\chi_M T$ product is 3.74 emu K mol^{-1}, due to the significant orbital contribution to the paramagnetism of HS iron(II) complexes and in line with previous findings on similar derivatives.[19] On cooling, it remains almost unvaried until 60 K, when it starts to decrease slowly and then abruptly below 20 K reaching 0.52 emu K mol^{-1} at 1.8 K. This behaviour reflects the selective population of the HS (S = 2) state, with zero field splitting (*zfs*) effects being responsible for the $\chi_M T$ drop at low temperature. All data could be satisfactorily fitted with PHI program[55] according to the Hamiltonian presented in Eq. 1, where g is the Landé factor and D and E are the axial and transverse *zfs* parameters, respectively. The best-fit parameters so-obtained are: g = 2.24(1), D = 10.0(3) cm^{-1} and E = 2.5(2) cm^{-1}. These values are in line with those previously reported for this class of compounds.[19]

$$\hat{H}_S = D\hat{S}_z^2 + E\left(\hat{S}_x^2 - \hat{S}_y^2\right) + \mu_B g\hat{\mathbf{B}} \cdot \hat{\mathbf{S}} \qquad (1)$$

It is reported that, in nearly all cases, the HS→LS transition is accompanied by a small increase in ϕ but essentially no change in θ.[7] Since the latter is already above the threshold value for SCO while the former is lower than required, for the first time with this type of ligand we attempted to promote SCO by applying an external pressure, in order to induce a re-alignment of the two ligands and force ϕ to a value higher than 172°. The magnetic properties of **1** were then investigated under pressure up to 1.00 GPa in the 1.8–300 K and 0–7 T temperature and magnetic field ranges, respectively, on a polycrystalline sample loaded into a CuBe piston-cylinder pressure cell. The temperature dependence of the $\chi_M T$ product at H_{DC} = 0.1 T and under pressure (ESI, Fig. S3†) is not much different from that observed under ambient pressure in a regular measurement (slight differences are due to small distortions of the raw data by the pressure cell body). The field dependence of the magnetization at 1.8 K (ESI, Fig. S3†) also does not deviate significantly from that measured under ambient pressure in a regular sample holder. This indicates that external pressures as high as 1.00 GPa have little or no influence on the magnetic properties of **1**, which does not undergo pressure-induced thermal SCO. The induction of SCO in **1** by compression would

Dalton Transactions Accepted Manuscript

View Article Online
DOI: 10.1039/C7DT00248C

Published on 22 February 2017. Downloaded by Fudan University on 22/02/2017 11:06:05.

presumably require a profound rearrangement of the two bpp-COOMe ligands around the iron(II) centre towards an N{py}–Fe–N{py} angle ϕ closer to 180°, but crystal packing and the position of the perchlorate anions probably hamper such a reorganization.

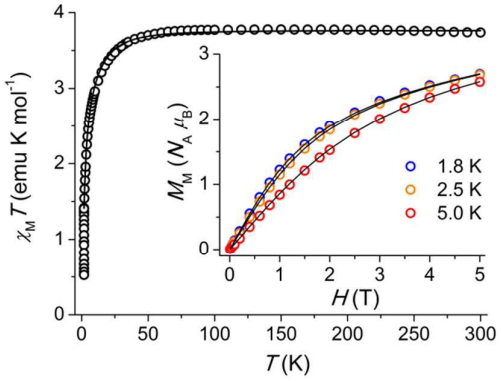

Fig. 3. Temperature dependence of the $\chi_M T$ product (black circles) for **1**; inset: field dependence of the molar magnetization, M_M, at 1.8, 2.5 and 5.0 K. Solid lines are given by the best-fit parameters (see text).

The temperature dependence of the low-field $\chi_M T$ product of **2** is reported in Fig. 4. Below 300 K, $\chi_M T$ values are close to zero, as expected for a fully populated LS state with a minor fraction of non-converted HS state (about 3%), as confirmed by isothermal magnetization profiles (ESI, Fig. S4†). Heating the compound above 300 K produces a sharp increase of $\chi_M T$, which reaches 1.11 emu K mol^{-1} at 400 K. Since complete population of the HS state would lead to a $\chi_M T$ value of 3.1–3.8 emu K mol^{-1}, approximately one third of the overall iron(II) content has undergone the spin transition at 400 K. By extrapolation, $T_{½}$ is expected to lie above 400 K, as observed in other SCO materials:[56,57] such a high temperature of spin transition hampers the observation of thermal hysteretic behaviour.

Due to the selective population of LS state at low temperature, the photo-magnetic activity of **2** was checked by means of light-dependent magnetization measurements. The compound was irradiated at 10 K with a 532 nm laser beam for approximately 2 h, till photo-stationary was reached with a recorded $\chi_M T$ value of 0.43 emu K mol^{-1}. Taking **1** as HS reference, this value corresponds to a HS fraction of about 12% (ESI, Fig. S5†). Partial photo-conversion in SCO systems is usually attributed to light penetration issues in the whole amount of the sample or to fast competing relaxation pathways available even at cryogenic temperatures. The latter may be related to spectral overlap of the photo-excitation/de-excitation bands, or to strong vibronic coupling between the

Dalton Transactions Accepted Manuscript

View Article Online
DOI: 10.1039/C7DT00248C

Published on 22 February 2017. Downloaded by Fudan University on 22/02/2017 11:06:05.

metastable HS and the ground LS states (adiabatic phonon relaxation), as suggested by the high temperature of SCO interconversion.[58]

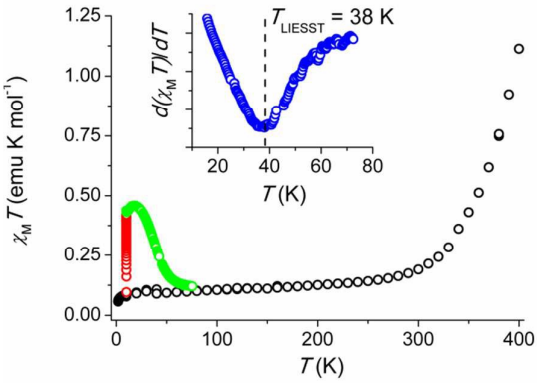

Fig. 4 Temperature dependence of the $\chi_M T$ product between 1.8 and 400 K of **2** in the dark (black circles), under irradiation with 532-nm light at 10 K (red circles) and upon heating after irradiation (green circles); inset: determination of the T_{LIESST} value.

After switching the light off, the $\chi_M T$ plot was recorded (Fig. 4, green circles) as the temperature was gradually increased at a rate of 0.3 K min^{-1}, following standard T_{LIESST} protocol.[21,25,59] At first, the $\chi_M T$ plot increased due to the *zfs* of the photo-induced HS iron(II) ion and reached a maximum value of 0.46 emu K mol^{-1} forming a plateau from 16 to 20 K. Afterwards, a monotonic decrease of the $\chi_M T$ plot was observed upon warming up until the curve reached the values found without irradiation, at around 75 K. A T_{LIESST} value of 38 K was determined from the minimum of the $d\chi_M T/dT$-*vs*-T curve (Fig. 4, inset).

Theoretical calculations

Theoretical calculations on this kind of compounds have been reported in recent years,[60] aiming at describing the ground state,[61,62] the LIESST phenomenon[63] and the impact of crystal packing[62,64] on the spin state. The HS-LS dualism is here investigated through analysis of the energies and the atomic charges of the optimised structures of both ligands and complexes.

Geometry optimizations were performed on the cations $[Fe(bpp\text{-}R)_2]^{2+}$ in the gas phase, starting from the geometries experimentally found in the X-ray structures of **1** and **2**·MeCN and imposing the same spin configuration as determined by magnetic measurements (below 300 K for **2**), that is $S = 2$ for **1** and $S = 0$ for **2**. Calculations provided structural parameters in very close agreement with

Dalton Transactions Accepted Manuscript

View Article Online
DOI: 10.1039/C7DT00248C

Published on 22 February 2017. Downloaded by Fudan University on 22/02/2017 11:06:05.

the experimental ones (Tables 2 and 3), confirming that the two compounds occupy in the solid state two stable minima in their respective Potential Energy Surface (PES). In particular, the clear distinction between the distorted and the undistorted octahedral geometries shown by **1** and **2**·MeCN, respectively, has been accurately reproduced.

In the attempt to rationalize the different magnetic behaviour shown by **1** and **2**, and the mutual effect between their spin configuration and structural properties, geometry optimizations were performed also on the complexes in their opposite spin configurations (i.e., $S = 0$ for **1** and $S = 2$ for **2**), starting from the hypothetical undistorted and distorted geometries, respectively. Well defined minima have been obtained, where the geometry of complex **1** was similar to that of **2** at low spin and the geometry of complex **2** was similar to that of **1** at high spin (see last columns of Tables 2 and 3). For both compounds, the HS distorted structure was found to be more stable than the LS undistorted one by 13.2 (**1**) and 13.7 kcal mol^{-1} (**2**). These results indicate that intermolecular interactions, neglected in the present gas-phase calculations, should be responsible for the unexpected stabilization of the LS structure observed for **2** in the solid state at temperatures below 400 K. In fact, **1** shows only weak C–H···O interactions in its crystal structure and assumes the lowest energy configuration. By contrast, the network of relatively strong intermolecular H bonds in **2**·MeCN can favour the population of the relative minimum on its PES with respect to the absolute one.

Owing to the important role played by enthalpy and entropy contributions in determining the relative stability of the spin states of the complexes,[62,64] thermal analysis at 298 K was also performed. While the same $\Delta G_{HS\rightarrow LS}$ free energy variation from the distorted HS to the undistorted LS state was obtained for **1** and **2** (16.3 kcal mol^{-1}), a slightly larger enthalpy variation was obtained for **2** with respect to **1** ($\Delta H_{HS\rightarrow LS}$ = 13.2 vs. 11.3 kcal mol^{-1}, respectively), suggesting an even stronger impact of crystal packing in stabilizing the LS state for **2**.

Plots of the frontier Molecular Orbitals (MOs) mainly localized on the iron(II) centre are reported in ESI, Fig. S6† together with the corresponding energies and the *d*-orbital contributions. By considering the unoccupied and the doubly or singly occupied MOs closest in energy, we computed energy gaps equal to 134.97 and 72.28 kcal mol^{-1} for the LS and the HS states of **1** and 135.04 and 73.94 kcal mol^{-1} for the corresponding states of **2**. Such quantities can be related to the ligand field strengths at the iron(II) ion, 10Dq, providing $10Dq^{LS}/10Dq^{HS}$ ratios equal to 1.87 and 1.83 for **1** and **2**, respectively. These results are in agreement with the relationship proposed by Halcrow *et al.*,[18] who connected $10Dq^{LS}/10Dq^{HS}$ with the sixth power of the average Fe–N bond length ratios in the HS and LS states, $(r_{HS}/r_{LS})^6$, equal to 1.82 and 1.81 for **1** and **2**, respectively

Dalton Transactions Accepted Manuscript

View Article Online
DOI: 10.1039/C7DT00248C

Published on 22 February 2017. Downloaded by Fudan University on 22/02/2017 11:06:05.

(Tables 2 ad 3). Moreover, such ratios are significantly greater than 1.74, the value typically observed for compounds showing SCO,[3] further confirming that at molecular level both compounds share the same behaviour without any expected SCO transition.

The atomic charges of the four optimized structures and of the free ligands were determined through NBO analysis,[47] following an approach of demonstrated validity[66] (ESI, Table S3†). In the two free ligands, the overall charge of the R groups is close to zero, implying that the substituents do not affect the charge distribution in the bpp backbone. By consequence, the three nitrogen atoms involved in the coordination to the metal have the same negative charges in the two cases, with the pyridyl nitrogen atom more negative (–0.42 e) than the pyrazolyl ones (about –0.26 e). The two ligands are thus expected to exhibit comparable donor power to the iron(II) centre. Irrespective to the R substituent, the residual charge on the metal is indeed close to zero in the LS state or +0.91 e in the HS state. Furthermore, the residual charge of the COOMe and triolH_3 groups in all cases remains low and almost constant (0.10–0.12 e). This analysis indicates a similar effect of ligand electronic character on the coordination geometry.

Discussion

Computational analysis on the gas-phase cations $[Fe(bpp\text{-}R)_2]^{2+}$ of **1** and **2** indicates that in both cases the HS configuration is the most stable one, even including temperature effects. The two bpp-COOMe and bpp-triolH_3 ligands appear to exert comparable electronic influence on the spin state of the iron(II) ion, as evidenced by quite similar computed charges and geometrical parameters when the same spin configuration is considered (compare data of columns HS (S = 2) and those of columns LS (S = 0) in Tables 2 and 3). It then results that the different magnetic behaviour of **1** and **2** observed in the solid state should be ascribed to the different patterns of intermolecular interactions in their crystal structures. Taking into account similar anion-cation electrostatic attractions due to the use of perchlorate in both compounds,[64] H bonds are the main structural motif differentiating the two structures from each other. Relatively strong[67] O–H···O bonds connect molecules of **2** on either sides forming linear, infinite chains that develop approximately parallel to the N{py}–Fe–N{py} bond direction. The almost optimal arrangement of H bonds along these chains (O–H···O angle measures 163.0°) is possible only with a concomitant N{py}–Fe–N{py} angle ϕ close to 180°, a geometry which promotes the LS configuration of the metal ion. This would suggest that H bonding can be considered as the driving force for the adoption of a LS

Dalton Transactions Accepted Manuscript

View Article Online
DOI: 10.1039/C7DT00248C

Published on 22 February 2017. Downloaded by Fudan University on 22/02/2017 11:06:05.

configuration by **2**, until the entropy-driven stabilization of the HS state sets in at sufficiently high temperatures.

A scenario similar to the one observed in **2** holds in two other members of the $[Fe(bpp\text{-}R)_2](X)_2$ family, namely $[Fe(bpp\text{-}pPy)_2H](ClO_4)_3$[27] and $[Fe(bpp\text{-}COOH)_2](ClO_4)_2$.[31] In the former, the complex cations are arranged in supramolecular chains through $(N–H)^+\cdots N$ hydrogen bonds involving the 4-Py substituents (N···N = 2.654 Å). Distortion angles are $\phi = 174.9°$ and $\theta = 87.2°$ and the compound displays a 2-K wide thermal hysteresis loop with $T_{½\uparrow}$ = 287 K and $T_{½\downarrow}$ = 285 K.[27] In $[Fe(bpp\text{-}COOH)_2](ClO_4)_2$, a chain-like supramolecular structure is also attained via a pair of complementary H bond interactions between 4-carboxylic groups (O···O = 2.671 Å). In this case, distortion angles ($\phi = 180°$ and $\theta = 87°$) are within 1° from those we found in **2** and the compound also exhibits SCO above room temperature, with $T_{½\uparrow}$ = 384 K, $T_{½\downarrow}$ = 381 K and T_{LIESST} = 60 K.[31] The lower T_{LIESST} observed in **2** (38 K) suggests a decrease in the thermal activation barrier to the relaxation of the metastable HS phase. This finding, along with the lower photo-converted HS fraction at low temperature and the higher $T_{½}$, fits into the Inverse Gap Energy Law introduced by Hauser[58] and points out a high energy difference between the two isomeric spin forms of **2**. Interestingly, the organization of deprotonated $[Fe(bpp\text{-}triol)_2]^{4–}$ units into 1D chains with $[MnMo_6O_{18}]^{3+}$ polyoxometallate (POM) fragments was found to further increase $T_{½}$, leading to a stable LS configuration up to 400 K, with a similar effect as H bonds.[49] Unfortunately, no X-ray structural data are available for this hybrid compound.

Compound **1** can be also compared with $[Fe(bpp\text{-}COOH)_2](ClO_4)_2$[31] and $[Fe(bpp\text{-}Me)_2](ClO_4)$.[22] Once the possibility to form H-bonded 1D chains is removed via esterification of the carboxylic fragment, the weak C–H···O/π intermolecular interactions in the crystal packing of **1** lead to a very distorted cation, which is then stabilised in the HS state at all temperatures. $[Fe(bpp\text{-}Me)_2](ClO_4)$[22] features secondary interactions similar to **1**, but the lower steric hindrance of the methyl group leads to a 'terpyridine embrace packing' of the cations and then thermally-induced HS↔LS conversion.

Conclusions

The present work describes two new members of the $[Fe(bpp\text{-}R)_2](X)_2$ family, which reside well in the overall mosaic drawn by Halcrow *et al.* for this class of compounds (see Fig. 5 for a ϕ vs. θ plot based on the available X-ray structural data,[7,8,22,26,31] including those for **1** and **2**). It also adds important insights into the role of intermolecular contacts in promoting and modulating spin conversion. Although the two ligands display the same donor power to the iron(II) centre, as

Dalton Transactions Accepted Manuscript

View Article Online
DOI: 10.1039/C7DT00248C

Published on 22 February 2017. Downloaded by Fudan University on 22/02/2017 11:06:05.

outlined by NBO charges, **1** (R = COOMe) possesses a heavily-distorted octahedral coordination environment (ϕ = 158.77(5)° and θ = 80.738(12)°) that hampers the SCO from its thermodynamic HS state, even under applied pressure. On the other side, **2** (R = triolH_3) features a much more regular coordination sphere (ϕ = 179.30(15)° and θ = 87.414(34)°) and a LS state up to 400 K, when a thermally induced SCO sets in; at cryogenic temperatures, **2** displays photo-magnetic properties through LIESST effect with T_{LIESST} = 38 K.

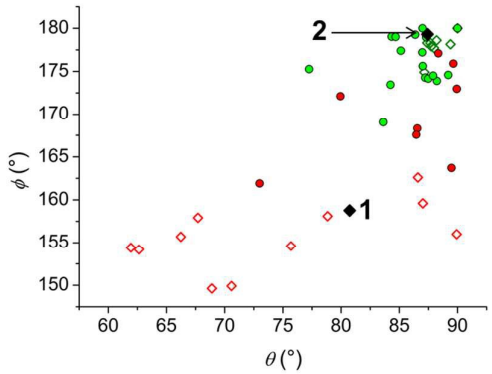

Fig. 5 Plot of the values of θ vs. ϕ from the [Fe(bpp-R)$_2$](X)$_2$ compounds for HS (◇) and LS (◇) complexes that remain in that spin state at all tested temperatures, and for complexes in their HS (●) or LS (●) state which undergo SCO upon cooling or heating, respectively. When more than one independent molecule is present in the crystal structure, the mean value is reported as unique point. Compounds subject of the present paper are highlighted as filled black diamonds (◆).

Since our theoretical studies indicate that both complexes have a thermodynamic HS state in the gas phase, intermolecular interactions must provide the supplementary energy contribution necessary to invert the stability of the spin configurations and afford a LS state in **2** below 400 K. In the solid state, the [Fe(bpp-triolH_3)$_2$]$^{2+}$ cations are indeed involved in a network of relatively strong H bonds with the formation of infinite chains through O–H···O contacts and the presence of interchain N–H···O linkages. This approach stresses out the idea that SCO behaviour can be actively modulated by functionalization of the ligands without directly affecting their coordination towards the iron(II) centre, but simply exploiting their potential in giving specific intermolecular interactions. Furthermore, as a certain aim in our future research, the triolH_3 fragment can act as tripodal ligand for the well-known propeller-like Fe_4 SMMs[68] and afford multi-responsive compounds similar to the bimetallic Mn^{III}-Fe^{II} 1D chains comprising alternating POMs and SCO centres recently reported.[49]

Dalton Transactions Accepted Manuscript

View Article Online
DOI: 10.1039/C7DT00248C

Published on 22 February 2017. Downloaded by Fudan University on 22/02/2017 11:06:05.

Dalton Transactions Accepted Manuscript

Acknowledgments

The research has been supported by the Italian MIUR through the FIRB project no. RBAP117RWN and by the European Research Council through the Advanced Grant MolNanoMaS no. 267746. D. P. gratefully acknowledges the financial support of the Polish Ministry of Science and Higher Education within the Iuventus Plus Programme, grant agreement no. 0370/IP3/2015/73. Authors also thanks Prof. Roberta Sessoli (Dipartimento di Chimica 'Ugo Schiff', Università degli Studi di Firenze) for the helpful discussion.

References

1 a) M. A. Halcrow (Ed.), *Spin-Crossover Materials – Properties and Applications*, Wiley, Chichester, 2013; b) J. F. Letard, P. Guionneau and L. Goux-Capes, *Spin Crossover in Transition Metal Compounds III, Top. Curr. Chem.* 2004, **235**, 221–249; c) P. Guionneau, M. Marchivie, G. Bravic, J. F. Letard and D. Chasseau, *Spin Crossover in Transition Metal Compounds II, Top. Curr. Chem.*, 2004, **234**, 97–128.

2 a) O. Sato, J. Tao and Y.-Z. Zhang, *Angew. Chem. Int. Ed.*, 2007, **46**, 2152–2187; b) H. J. Shepherd, G. Molnár, W. Nicolazzi, L. Salmon and A. Bousseksou, *Eur. J. Inorg. Chem.*, 2013, 653–661.

3 a) P. Gütlich and A. Hauser, *Coord. Chem. Rev.*, 1990, **97**, 1–22; b) P. Gutlich, A. Hauser and H. Spiering, *Angew. Chem. Int. Ed. Eng.*, 1994, **33**, 2024–2054.

4 M. A. Halcrow, *Chem. Lett.*, 2014, **43**, 1178–1188.

5 P. Gütlich, A. B. Gaspar and Y. Garcia, *Beilstein J. Org. Chem.*, 2013, **9**, 342–391.

6 P. Gutlich, Y. Garcia and H. A. Goodwin, *Chem. Soc. Rev.*, 2000, **29**, 419–427.

7 M. A. Halcrow, *Coord. Chem. Rev.*, 2009, **253**, 2493–2514.

8 L. J. Kershaw Cook, R. Mohammed, G. Sherborne, T. D. Roberts, S. Alvarez and M. A. Halcrow, *Coord. Chem. Rev.*, 2015, **289–290**, 2–12.

9 S. Hayami, Z. Z. Gu, M. Shiro, Y. Einaga, A. Fujishima and O. Sato, *J. Am. Chem. Soc.*, 2000, **122**, 7126–7127.

10 N. Bridonneau, J. Long, J. L. Cantin, J. von Bardeleben, S. Pillet, E. E. Bendeif, D. Aravena, E. Ruiz and V. Marvaud, *Chem. Commun.*, 2015, **51**, 8229–8232.

11 D. Pinkowicz, M. Rams, M. Misek, K. V. Kamenev, H. Tomkowiak, A. Katrusiak and B. Sieklucka, *J. Am. Chem. Soc.*, 2015, **137**, 8795–8802.

View Article Online
DOI: 10.1039/C7DT00248C

Published on 22 February 2017. Downloaded by Fudan University on 22/02/2017 11:06:05.

12 P. Gütlich, V. Ksenofontov and A. B. Gaspar, *Coord. Chem. Rev.*, 2005, **249**, 1811–1829.

13 V. Ksenofontov, A. B. Gaspar, J. A. Real and P. Gütlich, *J. Phys. Chem. B*, 2001, **105**, 12266–12271.

14 M. A. Halcrow, *New J. Chem.*, 2014, **38**, 1868–1882.

15 J. Olguin and S. Brooker, *Coord. Chem. Rev.*, 2011, **255**, 203–240.

16 in reference 8, Halcrow *et al*. refer to the clamp angle as φ, that is actually the same greek letter as ϕ; in order to avoid confusion we preferred to change the symbol to ψ.

17 M. A. Halcrow, *Chem. Soc. Rev.*, 2011, **40**, 4119–4142.

18 J. M. Holland, J. A. McAllister, C. A. Kilner, M. Thornton-Pett, A. J. Bridgeman and M. A. Halcrow, *J. Chem. Soc., Dalton Trans.*, 2002, 548–554.

19 J. Elhaïk, D. J. Evans, C. A. Kilner and M. A. Halcrow, *Dalton Trans.*, 2005, 1693–1700.

20 V. A. Money, J. S. Costa, S. Marcen, G. Chastanet, J. Elhaik, M. A. Halcrow, J. A. K. Howard and J. F. Letard, *Chem. Phys. Lett.*, 2004, **391**, 273–277.

21 S. Marcen, L. Lecren, L. Capes, H. A. Goodwin and J. F. Letard, *Chem. Phys. Lett.*, 2002, **358**, 87–95.

22 L. J. Kershaw Cook, F. L. Thorp-Greenwood, T. P. Comyn, O. Cespedes, G. Chastanet and M. A. Halcrow, *Inorg. Chem.,* 2015, **54**, 6319–6330.

23 N. T. Nadhu, I. Salistros, F. Schramm, S. Klyatskaya, O. Fuhr and M. Ruben, *C. R. Chimie*, 2008, **11**, 1166–1174.

24 L. J. Kershaw Cook, H. J. Shepard, T. P. Comyn, C. Baldé, O. Cespedes, G. Chastanet and M. A. Halcrow, *Chem. Eur. J.*, 2015, **21**, 4805–4816.

25 a) C. Carbonera, J. S. Costa, V. A. Money, J. Elhaik, J. A. K. Howard, M. A. Halcrow and J. F. Letard, *Dalton Trans.*, 2006, 3058–3066; b) V. A. Money, J. Elhaïk, M. A. Halcrow and J. A. K. Howard, *Dalton Trans.*, 2004, 1516–1518.

26 L. J. Kershaw Cook, R. Kulmaczewski, O. Cespedes and M. A. Halcrow, *Chem. Eur. J.*, 2016, **22**, 1789–1799.

27 C. Rajadurai, F. Schramm, S. Brink, O. Fuhr, M. Ghafari, R. Kruk and M. Ruben, *Inorg. Chem.*, 2006, **45**, 10019–10021.

28 I. Salistros, J. Pavlik, R. Boča, O. Fuhr, C. Rajadurai and M. Ruben, *CrystEngComm*, 2010, **12**, 2361–2368.

29 I. Šalistroš, O. Fuhr, R. Kruk, Ján Pavlik, L. Pogány, B. Schäfer, M. Tatarko, R. Boča, W. Linert and M. Ruben, *Eur. J. Inorg. Chem.*, 2013, 1049–1057.

Dalton Transactions Accepted Manuscript

View Article Online
DOI: 10.1039/C7DT00248C

Published on 22 February 2017. Downloaded by Fudan University on 22/02/2017 11:06:05.

30 C. Rajadurai, Z. Qu, O. Fuhr, B. Gopalan, R. Kruk, M. Ghafari and M. Ruben, *Dalton Trans.*, 2007, 3531–3537.

31 A. Abhervé, M. Clemente-Leon, E. Coronado, C. J. Gomez-Garcia and M. Lopez-Jorda, *Dalton Trans.*, 2014, **43**, 9406–9409.

32 M. Nihei, I. Han, H. Tahira and H. Oshio, *Inorg. Chim. Acta*, 2008, **361**, 3926–3930.

33 J. Elhaïk, C. M. Pask, C. A. Kilner and M. A. Halcrow, *Tetrahedron*, 2007, **63**, 291–298.

34 M. Nihei, N. Takahashi, H. Nishikawa and H. Oshio, *Dalton Trans.*, 2011, **40**, 2154–2156.

35 R. González-Prieto, B. Fleury, F. Schramm, G. Zoppellaro, R. Chandrasekar, O. Fuhr, S. Lebedkin, M. Kappes and M. Ruben, *Dalton Trans.*, 2011, **40**, 7564–7570.

36 a) I. Šalitroš, O. Fuhr, A. Eichhöfer, R. Kruk, Ján Pavlik, L. Dlháň, R. Boča and M. Ruben, *Dalton Trans.*, 2012, **41**, 5163–5171; b) I. Šalitroš, L. Pogány, M. Ruben, R. Boča and W. Linert, *Dalton Trans.*, 2014, **43**, 16584–16587; c) I. Šalitroš, O. Fuhr, and M. Ruben, *Materials*, 2016, **9**, 585–594.

37 M. Nihei, T. Maeshima, Y. Kose and H. Oshio, *Polyhedron*, 2007, **26**, 1993–1996.

38 a) Y. Hasegawa, K. Takahashi, S. Kume and H. Nishihara, *Chem. Commun.*, 2011, **47**, 6846–6848; b) K. Takahashi, Y. Hagesawa, R. Sakamoto, M. Nishikawa, S. Kume, E. Nishibori and H. Nishihara, *Inorg. Chem.* 2012, **51**, 5188–5198; c) Y. Hagesawa, R. Sakamoto, K. Takahashi and H. Nishihara, *Inorg. Chem.* 2013, **52**, 1658–1665.

39 L. J. Kershaw Cook, R. Kulmaczewski, R. Mohammed, S. Dudley, S. A. Barrett, M. A. Little, R. J. Deeth and M. A. Halcrow, *Angew. Chem. Int. Ed.*, 2016, **55**, 4327–4331.

40 A. Altomare, G. Cascarano, C. Giacovazzo and A. Guagliardi, *J. Appl. Crystallogr.*, 1993, **26**, 343–350.

41 G. M. Sheldrick, *Acta Cryst. Sect. C: Struct. Chem.*, 2015, **C71**, 3–8.

42 L. J. Farrugia, *J. Appl. Crystallogr.*, 2012, **45**, 849–854.

43 C. F. Macrae, I. J. Bruno, J. A. Chisholm, P. R. Edgington, P. McCabe, E. Pidcock, L. Rodriguez-Monge, R. Taylor, J. van de Streek and P. A. Wood, *J. Appl. Crystallogr.*, 2008, **41**, 466–470.

44 G. A. Bain and J. F. Berry, *J. Chem. Educ.*, 2008**, 85**, 532−536.

45 Gaussian 09, Revision D.01, M. J. Frisch, G. W. Trucks, H. B. Schlegel, G. E. Scuseria, M. A. Robb, J. R. Cheeseman, G. Scalmani, V. Barone, B. Mennucci, G. A. Petersson, H. Nakatsuji, M. Caricato, X. Li, H. P. Hratchian, A. F. Izmaylov, J. Bloino, G. Zheng, J. L. Sonnenberg, M. Hada, M. Ehara, K. Toyota, R. Fukuda, J. Hasegawa, M. Ishida, T. Nakajima, Y. Honda, O. Kitao, H. Nakai, T. Vreven, J. A. Jr. Montgomery, J. E. Peralta, F.

Dalton Transactions Accepted Manuscript

View Article Online
DOI: 10.1039/C7DT00248C

Published on 22 February 2017. Downloaded by Fudan University on 22/02/2017 11:06:05.

Ogliaro, M. Bearpark, J. J. Heyd, E. Brothers, K. N. Kudin, V. N. Staroverov, R. Kobayashi, J. Normand, K. Raghavachari, A. Rendell, J. C. Burant, S. S. Iyengar, J. Tomasi, M. Cossi, N. Rega, J. M. Millam, M. Klene, J. E. Knox, J. B. Cross, V. Bakken, C. Adamo, J. Jaramillo, R. Gomperts, R. E. Stratmann, O. Yazyev, A. J. Austin, R. Cammi, C. Pomelli, J. W. Ochterski, R. L. Martin, K. Morokuma, V. G. Zakrzewski, G. A. Voth, P. Salvador, J. J. Dannenberg, S. Dapprich, A. D. Daniels, Ö. Farkas, J. B. Foresman, J. V. Ortiz, J. Cioslowski and D. J. Fox, Gaussian, Inc., Wallingford CT, 2013.

46 Y. Zhao and D. Truhlar, *Theo. Chem. Accounts*, 2008, **120**, 215.

47 a) A. E. Reed and F. Weinhold, *J. Chem. Phys.*, 1985, **83**, 1736–1740; b) A. E. Reed, L. A. Curtiss and F. Weinhold, *Chem. Rev.*, 1988, **88**, 899–926.

48 M. A. Halcrow, *Coord. Chem. Rev.*, 2005, **249**, 2880–2908.

49 A. Abhervé, M. Palacios-Corella, J. M. Clemente-Juan, R. Marx, P. Neugebauer, J. van Slageren, M. Clemente-Leon and E. Coronado, *J. Mater. Chem. C*, 2015, **3**, 7936–7945.

50 M. Adamczyk, S. R. Akireddy and R. E. Reddy, *Tetrahedron*, 2002, **58**, 6951–6963.

51 C. Klein, E. Baranoff, M. Graetzel and M. K. Nazeeruddin, *Tetrahedron Letters*, 2011, **52**, 584–587.

52 J. Leblond, H. Gao, A. Petitjean and J.-C. Leroux, *J. Am. Chem. Soc.*, 2010, **132**, 8544–8545.

53 J. V. Mello and N. S. Finney, *Organic Letters*, 2001, **3**, 4263–4265.

54 L. Rigamonti, A. Cinti, A. Forni, A. Pasini and O. Piovesana, *Eur. J. Inorg. Chem.*, 2008, 3633–3647.

55 N. F. Chilton, R. P. Anderson, L. D. Turner, A. Soncini and K. S. Murray, *J. Comput. Chem.*, 2013, **34**, 1164–1175.

56 X. Bao, P.-H. Guo, W. Liu, J. Tucek, W.-X. Zhang, J.-D. Leng, X.-M. Chen, I. Y. Gural'skiy, L. Salmon, A. Bousseksou and M.-L. Tong, *Chem. Sci.*, 2012, **3**, 1629–1633.

57 G. S. Matouzenko, S. A. Borshch, E. Jeanneau and M. B. Bushuev, *Chem. Eur. J.*, 2009, **15**, 1252–1260.

58 A. Hauser, *Spin Crossover in Transition Metal Compounds II*, *Top. Curr. Chem.,* 2004, **234**, 155–198.

59 J. F. Letard, P. Guionneau, O. Nguyen, J. S. Costa, S. Marcen, G. Chastanet, M. Marchivie and L. Goux-Capes, *Chem. Eur. J.*, 2005, **11**, 4582–4589.

60 S. Vela, M. Fumanal, J. Ribas-Ariño and V. Robert, *J. Comput. Chem.*, 2016, **37**, 947–953.

Dalton Transactions Accepted Manuscript

View Article Online
DOI: 10.1039/C7DT00248C

61 N. Suaud, M.-L. Bonnet, C. Boilleau, P. Labèguerie and N. Guihéry, *J. Am. Chem. Soc.*, 2009, **131**, 715–722.

62 S. Vela, M. Fumanal, J. Ribas-Arino and V. Robert, *Phys. Chem. Chem. Phys.*, 2015, **17**, 16306–16314.

63 A. Droghetti, D. Alfè and S. Sanvito, *Phys. Rev. B*, 2013, **87**, 205114.

64 S. Vela, J. J. Novoa and J. Ribas-Arino, *Phys. Chem. Chem. Phys.*, 2014, **16**, 27012–27024.

65 Torsion angles required for the Θ definition were calculated by considering the centroids of the triangular faces of the pseudo-octahedron.

66 L. Rigamonti, M. Rusconi, A. Forni and A. Pasini, *Dalton Trans.*, 2011, **40**, 10162–10173.

67 G. R. Desiraju and T. Steiner, The Weak Hydrogen Bond, OUP, Chichester, 1999.

68 a) A. Nava, L. Rigamonti, E. Zangrando, R. Sessoli, W. Wernsdorfer and A. Cornia, *Angew. Chem. Int. Ed.*, 2015, **54**, 8777–8782; b) L. Rigamonti, C. Cotton, A. Nava, H. Lang, T. Rüffer, M. Perfetti, L. Sorace, A.-L. Barra, Y. Lan, W. Wernsdorfer, R. Sessoli and A. Cornia, *Chem. Eur. J.*, 2016, **22**, 13705–13714.

Published on 22 February 2017. Downloaded by Fudan University on 22/02/2017 11:06:05.

Dalton Transactions Accepted Manuscript

View Article Online
DOI: 10.1039/C7DT00248C

Published on 22 February 2017. Downloaded by Fudan University on 22/02/2017 11:06:05.

Table of Contents

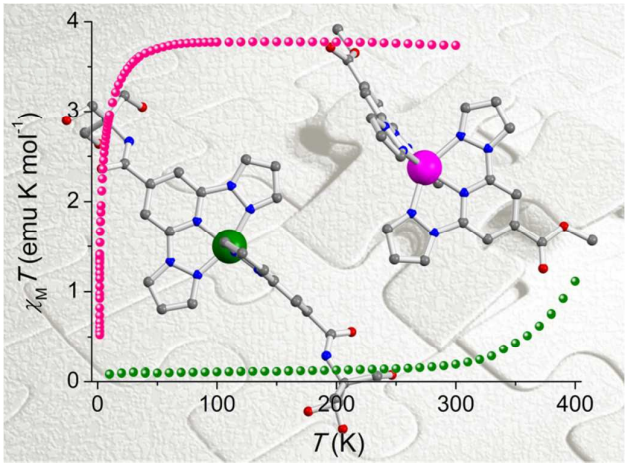

High or low spin state in iron(II) complexes with functionalised 2,6-bis(pyrazol-1-yl)pyridine ligands is efficaciously driven by intermolecular contacts.

Dalton Transactions Accepted Manuscript